PI semiactive control using MR dampers*

N. AGUIRRE**, F. IKHOUANE*** and J. RODELLAR†

** Department of Applied Mathematic III. School of Technical Industrial Engineering of Barcelona.
Technical University of Catalunya.
Urgell 187, 08036 Barcelona, Spain
E-mail: naile.aguirre@upc.edu

*** Department of Applied Mathematic III. School of Technical Industrial Engineering of Barcelona.
Technical University of Catalunya.
Urgell 187, 08036 Barcelona, Spain
E-mail: faical.ikhouane@upc.edu

† Department of Applied Mathematic III, Technical University of Catalunya.
Campus Nord C-2 08034 Barcelona, Spain
E-mail: jose.rodellar@upc.edu

Abstract

Magnetorheological (MR) dampers are a promising alternative structural active actuators as they provide adjustable damping over a wide range of frequencies without large power requirements. However, the complex dynamics that characterizes these devices makes it difficult to formulate control laws based on the MR damper model. Instead, many semiactive control strategies proposed in the literature have been based on the idea of ”clipping” the voltage signal so that the MR damper force ”tracks” a desired active control force which is computed on-line. With this idea many algorithms have been proposed using, among others, techniques such as optimal control, H_∞ control, sliding mode control, backstepping and QFT.

This work presents a semiactive control strategy based on the same idea of ”clipping” the voltage signal but using a simpler PI design. The proportional and integral gains of the controller are calculated so that the controller guarantees stability, minimization of the closed loop response and robustness against modeling errors. Effectiveness of the control strategy is compared to some others techniques and passive cases as well. Simulation results shows that this simple strategy can effectively improve the structural responses and achieve performance index comparable to that of more complex algorithms.

Key words : Semiactive control, MR dampers, PI control.

1. Introduction

MR damper technology have emeged as a promising way to protect structural systems from external hazards. MR dampers devices provide the structure with adjustable damping which is a function of a voltage signal. Hence, MR dampers based control combines the dissipative nature of passive systems with the adaptability of active ones without large power requirements.

However, the design of semiactive control strategies is not a simple task. In fact, it constitutes a very particular problem since, unlike active actuators, MR dampers can only provide the structure with dissipative forces which imposes a restriction in the control design. An approach commonly used in the literature is to compute an active force using a primary controller and then, look for a command voltage rule so that the MR damper friction force tracks the active one. The primary controller design has been designed using LQR/LQG [16],[19],[9],[8],[6],[4],[7],[32],[27],[17], modulated homogeneous friction [15],[16], sliding mode control [23],[26],[25],[30],

*Proceedings of MOVIC2010
August 17–20, 2010, Tokyo, Japan
(No. 10-010)

H_∞ control[20], dissipative-LQG[10], LMI/LQR[18], backstepping[29],[24],[36],[28],[34], QFT[35], [36],[34],[28], and velocity feedback[3], among others techniques.

These primary controllers are generally complex, and sometimes of difficult implementation because of either the number or complexity of measurements involved. The motivation of this work is to propose a simple control law with two measurements to achieve results comparable to those obtained by these complex controllers. We use the semiactive clipped technique with a PI primary controller. The gains of this controller are calculated so that the controller guarantees stability, minimization of the closed loop response and robustness against modeling errors. Numerical simulations are carried out to compare the effectiveness of this new controller to some others proposed in the literature.

The document is organized as follows: Section 2 deals with the mathematical representation of the controlled structure along with the modeling of the MR damper. Section 3 details the the semiactive control strategy by designing the active PI controller followed by the adjusting voltage rule. Section 4 define some performance index used to measure the control effectiveness. Then, Section 4 provide numerical results regarding to the effectiveness of the semiactive strategy when used for a structural system equipped with an MR damper. These results are compared to passive cases, active control and backstepping/QFT based control. Finally, conclusions are drawn in Section 5.

2. Formulation of the controlled system

2.1. Structural system

Consider a structural system with n floors equipped with a MR damper. Assuming that the structure is provided by a control force adequate to keep the response of the system in the linear region, equations of motion can be formulated as:

$$M\ddot{Q} + C\dot{Q} + KQ = -M\Gamma d + \Lambda f \tag{1}$$

where $Q = [x_1, x_2, \ldots, x_n]^T$, $\dot{Q} = [\dot{x}_1, \dot{x}_2, \ldots, \dot{x}_n]^T$ and $\ddot{Q} = [\ddot{x}_1, \ddot{x}_2, \ldots, \ddot{x}_n]^T$ correspond to the displacement, velocity and acceleration relative to the base, d is the ground acceleration relative to an inertial reference frame and f corresponds to the MR damper force.

Matrices M and K represent the mass and stiffness of the structure respectively

$$M = \text{diag}(m_i) \quad i = 1, ..., n$$

$$K = \begin{bmatrix} k_1 + k_2 & -k_2 & 0 & \cdots & \cdots & 0 \\ -k_2 & k_2 + k_3 & -k_3 & 0 & \cdots & \vdots \\ 0 & -k_3 & k_3 + k_4 & -k_4 & \ddots & \vdots \\ \vdots & 0 & -k_4 & \ddots & -k_{n-1} & 0 \\ \vdots & \vdots & \ddots & -k_{n-1} & k_{n-1} + k_n & -k_n \\ 0 & \cdots & \cdots & 0 & -k_n & k_n \end{bmatrix}$$

where m_i and k_i correspond respectively to mass and stiffness of the i–th floor.

Matrix C is the damping of the system computed by the method proposed in [5], [11] as follows

$$C = M\left(\sum_{i=1}^{n} \frac{2\zeta_i 2\pi f_{n_i}}{\phi_i^T M \phi_i} \phi_i \phi_i^T\right) M$$

where ϕ_i and f_{n_i} are eigenvectors and modal frequencies of $M^{-1}K$ so that $\Phi = [\phi_1, \phi_2 \cdots \phi_n]$ constitutes the modal matrix. Parameters ζ_i is the damping ratio associated to the i–th mode.

Vector $\Gamma = [1, 1, \cdots, 1]^T_{n\times 1}$ defines the influence of the external excitation d over the entire structural system and matrix $\Lambda_{n\times 1}$ sets the placement of the damper in the structure.

Equation (1) can be represented in the state space form as:

$$\dot{X} = A_s X + B_s f + E_s d \tag{2}$$

$$Z = C_z X + D_z f \tag{3}$$

$$y = C_y X + D_y f \tag{4}$$

$$A_s = \begin{bmatrix} 0_{n\times n} & I_{n\times n} \\ -M^{-1}K & -M^{-1}C \end{bmatrix}_{2n\times 2n} \quad B_s = \begin{bmatrix} 0_{n\times 1} \\ M^{-1}\Lambda \end{bmatrix}_{2n\times 1} \quad E_s = \begin{bmatrix} 0_{n\times 1} \\ -\Gamma \end{bmatrix}_{2n\times 1}$$

$$C_z = \begin{bmatrix} -M^{-1}K & -M^{-1}C \\ I_{n\times n} & 0_{n\times n} \end{bmatrix}_{2n\times 2n} \quad D_z = \begin{bmatrix} M^{-1}\Lambda \\ 0_{n\times 1} \end{bmatrix}_{2n\times 1}$$

$$C_y = A_1 \begin{bmatrix} -M^{-1}K & -M^{-1}C \end{bmatrix}_{n\times 2n} \quad D_y = A_1 \begin{bmatrix} M^{-1}\Lambda \end{bmatrix}_{n\times 1}$$

$$A_1 = \begin{bmatrix} 1 & 0_{1\times n-1} \end{bmatrix}_{1\times n}$$

where $X = [x_1, x_2, \ldots x_n, \dot{x}_1, \dot{x}_2, \ldots \dot{x}_n]^T$ is the state vector of the system, $y = \ddot{x}_{a_1}$ is the regulated output and $Z = [\ddot{x}_1, \ddot{x}_2, \ldots \ddot{x}_n, x_1, x_2, \ldots x_n]^T$. Variables x_i, $\dot{x}_i$ and $\ddot{x}_i$ are the relative displacement, velocity and acceleration of the floors respectively and $\ddot{x}_{a_1}$ is the absolute acceleration of the first floor.

The structure under study is the 3–story building referred in [33),(34)] which is equipped with a MR damper between the first and second floor as shown in Figure 1.

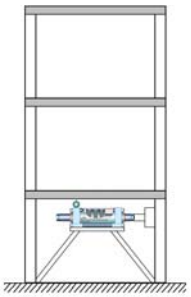

Fig. 1 3–story building equipped with a MR damper

The mass, stifnees and damping matrices for this system are taken as:

$$M = \begin{bmatrix} 202.53 & 0 & 0 \\ 0 & 202.53 & 0 \\ 0 & 0 & 202.53 \end{bmatrix} \frac{Ns^2}{cm} \tag{5}$$

$$K = \begin{bmatrix} 99320 & -56610 & 0 \\ -56610 & 113380 & -56610 \\ 0 & -56610 & 56610 \end{bmatrix} \frac{N}{cm} \tag{6}$$

$$C = \begin{bmatrix} 72.43 & -20.70 & 0 \\ -20.70 & 41.38 & -20.70 \\ 0 & 20.70 & 20.70 \end{bmatrix} \frac{Ns}{cm} \tag{7}$$

which correspond to fundamental frequencies

$$f_n = [1.09, 3.17, 4.74](\text{Hz}) \tag{8}$$

and damping ratios

$$\zeta = [0.31, 0.62, 0.63](\%). \tag{9}$$

The MR damper placement matrix is $\Lambda = [-1, 0, 0]^T$ and vector $\Gamma = [1, 1, 1]^T$.

2.2. MR damper

References[33),(34)] have used a small scale MR damper which is scaled to be incorporated into the large-scale structure from Figure 1. Then, MR damper force f is formulated as

$$f(t) = S_f f^*$$

where S_f is a scaling factor and f^* is the small scale MR damper force which is modeled using the modified version of the viscous + Dahl model referred in [13]. The viscous + Dahl model has been derived as a match point of the normalized version of the Bouc-Wen model [14] and the Bingham model[19] used to characterize MR dampers behaviour. This model has been successfully implemented to model full scale MR dampers as documented in [1].

It is formulated as:

$$f^*(t) = \kappa_x [v_{ic}(t)] \dot{x}_d(t) + \kappa_w [v_{ic}(t)] w(t) + \kappa_{xm} [v_{ic}(t)] x_d(t) \tag{10}$$

$$\dot{w}(t) = \rho (\dot{x}_d(t) - |\dot{x}_d(t)| w(t)) \tag{11}$$

where $\dot{x}_d(t) = \frac{\dot{x}_1(t)}{S_l}$ and $x_d(t) = \frac{x_1(t)}{S_l}$ are the velocity and displacement of the MR damper which corresponds to the first floor velocity and displacement scaled by factor S_l, $w(t)$ is an hysteretic variable (not accesible to measurements) that accounts for the hysteresis nonlinearity of the MR damper, ρ is a voltage–independent parameter and κ_x, κ_w, and κ_{xm} are voltage dependent parameters in the form

$$\kappa_x(v_{ic}) = \kappa_{x_a} + \kappa_{x_b} v_{ic} \tag{12}$$

$$\kappa_w(v_{ic}) = \kappa_{w_a} + \kappa_{w_b} v_{ic} \tag{13}$$

$$\kappa_{xm}(v_{ic}) = \kappa_{xm_a} + \kappa_{xm_b} v_{ic} \tag{14}$$

where κ_{x_a}, κ_{x_b}, κ_{w_a}, κ_{w_b}, κ_{xm_a}, and κ_{xm_b} are constant.

In addition, the current driver circuit of the MR damper introduces dynamics into the system. These dynamics are typically considered to be a first order time lag in the response of the device to changes in the command input. These dynamics are accounted for with the first order filter on the voltage given by

$$\dot{v}_{ic}(t) = -\eta(v_{ic}(t) - v(t)) \tag{15}$$

where $v(t)$ corresponds to the command voltage, v_{ic} is the actual voltage in the damper and $\frac{1}{\eta}$ is the time constant of this first order filter[31].

In references[33),(34)] damper force f^* is modeled by using the Bouc Wen model which can be easily transformed into the modified viscous + Dahl model (10)-(11). This comes straightforwardly from the fact that the viscous + Dahl model is a particular case of the normalized Bouc Wen model which, in turn, can reproduce exactly the same output of the Bouc Wen model as demonstrated in[13),(14)].

Thus, equivalences from the Bouc-Wen model parameters in [33),(34)] to the modified viscous + Dahl model parameters yields: $\kappa_{x_a} = 7.54$ (Ns/cm), $\kappa_{x_b} = 7.13$ (Ns/cm/V), $\kappa_{w_a} = 36.71$ (N), $\kappa_{w_b} = 201.54$(N/V), $\kappa_{xm_a} = 11.38$ (N/cm), $\kappa_{xm_b} = 14.44$ (N/cm/V) and $\rho = 92.85$ (cm^{-1}). Parameters $\eta = 57$ (s^{-1}), $V_{\max} = 5$ (V) and $f^*_{\max} = 3000$ (N).

3. Semiactive control strategy

Figure 2 shows the block diagram representation of the structural system in closed loop with the MR damper and the controller block.

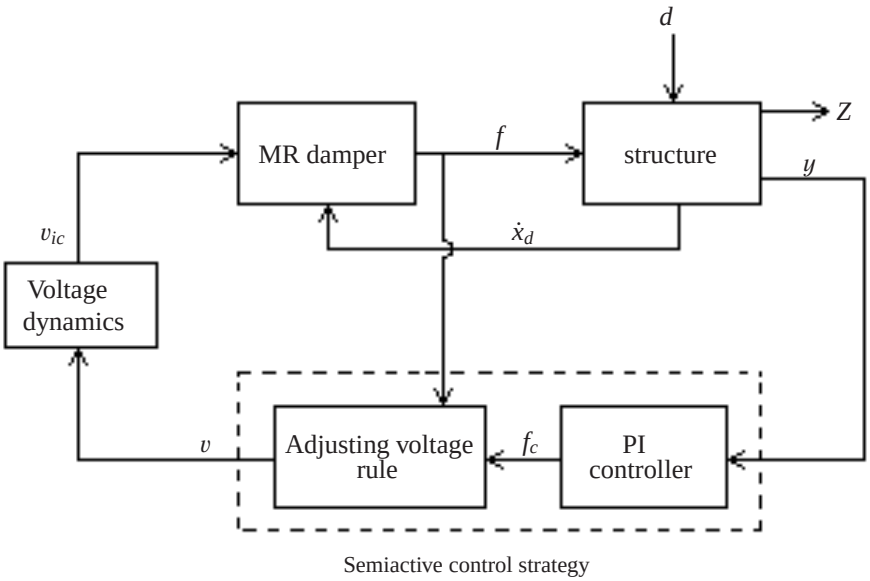

Fig. 2 Block diagram representation of the semiactive controlled system

It can be seen that the semiactive control strategy is divided in two blocks. The first block uses a PI controller to compute an active control force f_c. The second block implements an adjusting voltage rule to induce the MR damper force f to match as close as possible the control force f_c.

3.1. Control objectives

To design the PI controller, we consider the following assumption regarding to the external excitation $d(t)$:

Assumption 1: The function $d : [0, +\infty) \to \mathbb{R}$ is Lebesgue measurable. Moreover $\|d\|_\infty < \infty$ and, there exists some $\theta_t \in [0, +\infty)$ such that $d(t) = 0\ \forall t > \theta_t$.

Then our control objectives are:

When $d(t) \neq 0$, $\forall t \geq 0$ and for any initial conditions we have:

i. All the closed loop signals are bounded
ii. $\lim_{t\to\infty} y(t) = 0$ (output regulation).

When $d(t) \neq 0$, $\forall t \geq 0$ and for any initial conditions we have:

i. All the closed loop signals are bounded

The controller design is addressed in next section.

3.2. Control Design

PI control is a generic control loop feedback mechanism widely used in industrial control systems. This is not only due to its simple structure, which is conceptually easy to understand, but also to the fact that the algorithm provides adequate performance in many engineering applications[(2),(22)].

Consider the PI controller scheme shown in Figure 3. The PI controller calculates the error value e as the difference between the measured process variable y and the reference r, $e = r - y$.

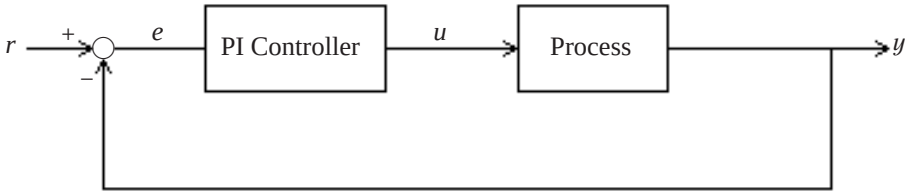

Fig. 3 Active control scheme with a PI controller

The control input u depends on the current and cumulative error weighted by parameters K_p and K_i respectively in the form

$$u(t) = K_p e(t) + K_i \int_0^t e(\tau) d\tau \tag{16}$$

where parameters K_p and K_i are the proportional and integral gains respectively. This is sketched in the block diagram form in Figure 4.

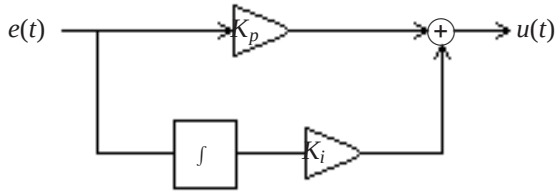

Fig. 4 Closed loop system

In the absence of disturbances, pure proportional control will retain a steady state error that is a function of the proportional gain and the process gain. However, the integral term takes into account the accumulated offset and eliminates the residual steady–state error that occurs with a proportional only controller.

Finally, as stability and performance of the PI controller depend on the selection of parameters K_p and K_i, they need to be tuned adequately. Many tuning methods have been proposed in the literature e.g., step and frequency response methods[(2),(12),(21),(37)]. However, they are mainly established for first and second order processes, and thus, are no longer valid for our puspose.

3.3. Synthesis of the active PI control

Figure 5 shows the block diagram representation of the system (2)-(4) where MR damper force f is substituted by an active force f_c which comes from a PI controller. Note that, according to our control objectives, reference signal has been set to zero which means that the proposed PI controller deal with a regulation problem.

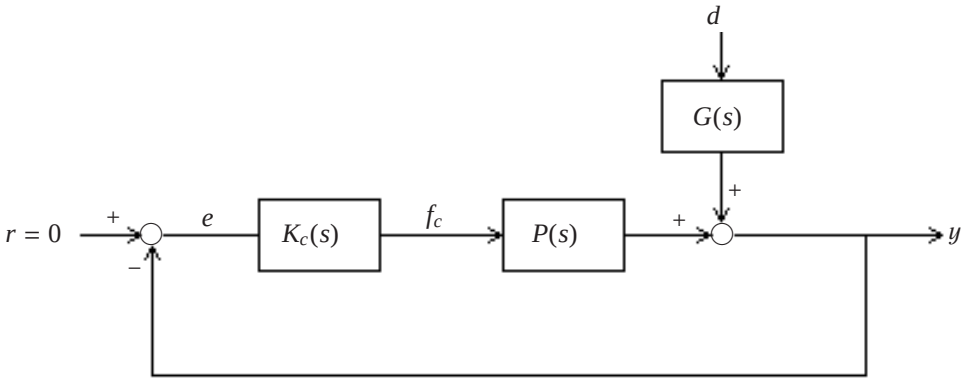

Fig. 5 Closed loop system - PI control

In this block diagram $r = 0$ represents the reference, $e = -y$ is the error signal, $K_c(s)$ is the transfer function of the PI controller which is expressed as

$$K_c(s) = \left(K_p + \frac{K_i}{s}\right), \tag{17}$$

$P(s)$ and $G(s)$ are the transfer functions from inputs f_c and d to output y respectively which are computed as

$$P(s) = C_y(sI - A_s)^{-1}B_s + D_y \tag{18}$$

$$G(s) = C_y(sI - A_s)^{-1}E_s \tag{19}$$

In our case, numerical values of these transfer functions are

$$P(s) = N_p(s)/D_p(s) \tag{20}$$

$$G(s) = N_g(s)/D_g(s) \tag{21}$$

where $N_p = -0.0049s^6 - 0.0015s^5 - 4.144s^4 - 0.2824s^3 - 386.9s^2$, $D_p = s^6 + 0.6642s^5 + 1330s^4 + 450.6s^3 + 4.118 \times 10^5 s^2 + 3.211 \times 10^4 s + 1.658 \times 10^7$, $N_g = 0.2554s^5 + 211s^4 + 279s^3 + 1.772 \times 10^5 s^2 + 3.211 \times 10^4 s + 1.658 \times 10^7$ and $D_g = s^6 + 0.6642s^5 + 1330s^4 + 450.6s^3 + 4.118 \times 10^5 s^2 + 3.211 \times 10^4 s + 1.658 \times 10^7$.

Let $\mathcal{L}(\cdot)$ be the Laplace–transform and define the following quantities:

$$\begin{aligned} Y(s) &= \mathcal{L}(y(t)) \\ D(s) &= \mathcal{L}(d(t)) \\ F_c(s) &= \mathcal{L}(f_c(t)) \end{aligned}$$

For zero initial conditions we get

$$Y(s) = P(s)F_c(s) + G(s)D(s) \tag{22}$$

where $F_c(s)$ is expressed as

$$F_c(s) = K_c(s)E(s) = -K_c(s)Y(s). \tag{23}$$

Substituting equations (17) and (23) into (22) we get

$$Y(s) = -P(s)\left(K_p + \frac{K_i}{s}\right)Y(s) + G(s)D(s) \tag{24}$$

which leads to

$$Y(s) = \frac{G(s)}{1 + P(s)(K_p + \frac{K_i}{s})}D(s). \tag{25}$$

Then, substituting (20)-(21) into equation (25) yields

$$Y(s) = \underbrace{\frac{N_g}{D_p + N_p K_p + s N_{p_0} K_i}}_{F(s)} D(s) \tag{26}$$

where N_{p_0} comes from factorization of polynomial N_p as $N_p = s^2 N_{p_0}$ and transfer function $F(s)$ account for the effect of the external excitation d into the regulated output y.

For nonzero initial conditions, the right–hand side of (26) has to be augmented by a term that take into account these initial conditions. This term translates into decaying exponentials in time domain. Since the perturbation $d(t) = 0 \; \forall t > \theta_t$, it follows that

$$\lim_{t \to \infty} y(t) = 0.$$

Similarly, it can be seen that for zero initial conditions, substitution of (26) into (23) gives:

$$F_c(s) = \frac{K_i N_g + s K_p N_g}{s\left[D_p + N_p K_p + s N_{p_0} K_i\right]} D(s) \tag{27}$$

For nonzero initial conditions, the right–hand side of (27) has to be augmented by a term that take into account these initial conditions. This term translates into decaying exponentials in time domain plus a constant term. Since the perturbation $d(t) = 0 \; \forall t > \theta_t$, it follows that

$$\lim_{t \to \infty} f_c(t) = f_{c_\infty} < \infty.$$

Therefore, in the interval $t \in [0, \theta_t]$ all closed loop signals are bounded due to the linearity of the system and controller. This implies that the control objective have been met.

From equation (26) it is clear that stability and performance of the controller depend on the values of parameters K_p and K_i. The next section addresses the issue of tuning these parameters.

3.3.1. PI tuning methodology Consider the (K_p, K_i)–plane where parameters K_p and K_i range from $-\infty$ to $+\infty$. The tuning procedure is proposed in terms of finding the optimal pair $(K_i, K_p)_{opt} \in (K_p, K_i)$–plane which guarantees system stability, minimization of the closed loop system response (equation (26)) and controller robustness against modeling errors.

Stability of the closed loop system

In this paragraph we look for a region $\Omega_1 \subseteq (K_p, K_i)$–plane where stability of the closed loop can be guaranteed.

From control system theory it is well known that the stability of the closed loop system relies on its characteristic equation. Thus, according to the general stability criterion, the closed loop system will be stable if and only if all of the roots of its characteristic equation, have negative real parts.

Consider the characteristic equation of our closed loop system, that is, the polynomial

$$A(s) = D_p + N_p K_p + N_{p_0} K_i s \tag{28}$$

from equation (26). It can be written as

$$A(s) = a_i s^i + a_{i-1} s^{i-1} + \cdots + a_0 s^0 \tag{29}$$

where coefficients a_i are functions of parameters K_p, K_i and coefficients of polynomials D_p, N_p and N_{p_0}.

Thus, stability of the closed loop system may be guaranteed by constraining polynomial $A(s)$ so that all of its roots have negative real parts. To this end, the Routh–Hurwitz stability criterion is invoked herein. This is very useful for us as it can determine whether any root of polynomial $A(s)$ have positive real parts without having to determine explicitly these roots.

This analytic technique based on Routh's array is illustrated in Table 1

s^n	a_n	a_{n-2}	a_{n-4}	$\cdots$
s^{n-1}	a_{n-1}	a_{n-3}	a_{n-5}	$\cdots$
s^{n-2}	b_1	b_2	b_3	$\cdots$
s^{n-3}	c_1	c_2	c_3	$\cdots$
$\vdots$	$\vdots$	$\vdots$	$\vdots$	$\vdots$
s^1				
s^0				

Table 1 Routh–Hurwitz stability criterion

where elements b_i, c_i and so on are computed as follows

$$b_1 = -\frac{1}{a_{n-1}}\begin{vmatrix} a_n & a_{n-2} \\ a_{n-1} & a_{n-3} \end{vmatrix} \quad b_2 = -\frac{1}{a_{n-1}}\begin{vmatrix} a_n & a_{n-4} \\ a_{n-1} & a_{n-5} \end{vmatrix} \quad \cdots$$

$$c_1 = -\frac{1}{b_1}\begin{vmatrix} a_{n-1} & a_{n-3} \\ b_1 & b_2 \end{vmatrix} \quad c_2 = -\frac{1}{b_1}\begin{vmatrix} a_{n-1} & a_{n-5} \\ b_1 & b_3 \end{vmatrix} \quad \cdots$$

This criterion states that a necessary and sufficient condition for all roots of polynomial $A(s)$ to have negative real parts is that all of the elements in the left column of the Routh's array have the same sign.

For our analysis, polynomial $A(s)$ is computed by substituting polynomials D_p, N_p and N_{p_0} from transfer functions (20)-(21) into (28) which gives

$$A(s) = a_6 s^6 + a_5 s^5 + a_4 s^4 + a_4 s^4 + a_3 s^3 + a_2 s^2 + a_1 s^1 + a_0 s^0 \tag{30}$$

where

$$a_6 = -0.0049K_p + 1 \tag{31}$$
$$a_5 = -0.0015K_p - 0.0049K_i + 0.6642 \tag{32}$$
$$a_4 = -4.144K_p - 0.0015K_i + 1330 \tag{33}$$
$$a_3 = -0.2824K_p - 4.144K_i + 450.6 \tag{34}$$
$$a_2 = -386.9K_p - 0.2824K_i + 4.118 \times 10^5 \tag{35}$$
$$a_1 = -386.9K_i + 3.211 \times 10^4 \tag{36}$$
$$a_0 = 1.658 \times 10^7 \tag{37}$$

The corresponding Routh–array is shown in Table 2

where

$$b_1 = \frac{a_4 a_5 - a_6 a_3}{a_5} \tag{38}$$
$$b_2 = \frac{a_2 a_5 - a_6 a_1}{a_5} \tag{39}$$
$$b_3 = a_0 \tag{40}$$
$$c_1 = \frac{a_3 b_1 - a_5 b_2}{b_1} \tag{41}$$
$$c_2 = \frac{a_1 b_1 - a_5 b_3}{b_1} \tag{42}$$

s^6	a_6	a_4	a_2	a_0
s^5	a_5	a_3	a_1	0
s^4	$-\frac{1}{a_5}\begin{vmatrix} a_6 & a_4 \\ a_5 & a_3 \end{vmatrix} = b_1$	$-\frac{1}{a_5}\begin{vmatrix} a_6 & a_2 \\ a_5 & a_1 \end{vmatrix} = b_2$	$-\frac{1}{a_5}\begin{vmatrix} a_6 & a_0 \\ a_5 & 0 \end{vmatrix} = b_3$	0
s^3	$-\frac{1}{b_1}\begin{vmatrix} a_5 & a_3 \\ b_1 & b_2 \end{vmatrix} = c_1$	$-\frac{1}{b_1}\begin{vmatrix} a_5 & a_1 \\ b_1 & b_3 \end{vmatrix} = c_2$	0	0
s^2	$-\frac{1}{c_1}\begin{vmatrix} b_1 & b_2 \\ c_1 & c_2 \end{vmatrix} = d_1$	$-\frac{1}{c_1}\begin{vmatrix} b_1 & b_3 \\ c_1 & 0 \end{vmatrix} = d_2$	0	0
s^1	$-\frac{1}{d_1}\begin{vmatrix} c_1 & c_2 \\ d_1 & d_2 \end{vmatrix} = e_1$	0	0	0
s^0	$-\frac{1}{e_1}\begin{vmatrix} d_1 & d_2 \\ e_1 & 0 \end{vmatrix} = f_1$	0	0	0

Table 2 Routh's array corresponding to polynomial 30.

$$d_1 = \frac{b_2 c_1 - b_1 c_2}{c_1} \tag{43}$$

$$d_2 = a_0 \tag{44}$$

$$e_1 = \frac{c_2 d_1 - c_1 d_2}{d_1} \tag{45}$$

$$f_1 = a_0 \tag{46}$$

Now, substituting (37) into (46) yields $f_1 = 1.658 \times 10^7 > 0$ which means that all other elements of the left column of the Routh's array must be positive. Thus, in our case, the Routh–Hurwitz stability criterion can be rendered into positiveness of terms a_6, a_5, b_1, c_1, d_1 and e_1.

Figure 6 illustrates how this requirement brings up some boundary conditions on parameters $K_p, K_i \in (K_p, K_i)$–plane corresponding to positiveness of every element in the left column of the Routh's array which is indicated by white areas. Finally, the region Ω_1 is obtained where Routh–Hurwitz stability criterion is satisfied and therefore, stability of the closed loop system is guaranteed.

Minimization of the closed loop system response

Once we have the stability region Ω_1, a region $\Omega_2 \subset \Omega_1$ is pursued in order to minimize the magnitude of the closed loop system response inside region Ω_1.

To this end, in equation (26), we consider that the input d is a sine waves with frequency ω_s. In steady–state, the output y is also a sine wave with frequency ω_s. Thus, equation (26) can be written as:

$$Y(jw) = F(jw) \cdot D(jw) \tag{47}$$

so that

$$|Y(jw)| \leq |F(jw)| \cdot |D(jw)| . \tag{48}$$

Consider the H_∞ norm of equation (47)

$$\|Y\|_\infty = \sup_{\omega \in (-\infty, \infty)} |Y(jw)| . \tag{49}$$

Applying the norm's triangle inequality yields

$$\|Y\|_\infty \leq \Upsilon \tag{50}$$

where

$$\Upsilon = \|F\|_\infty \|D\|_\infty . \tag{51}$$

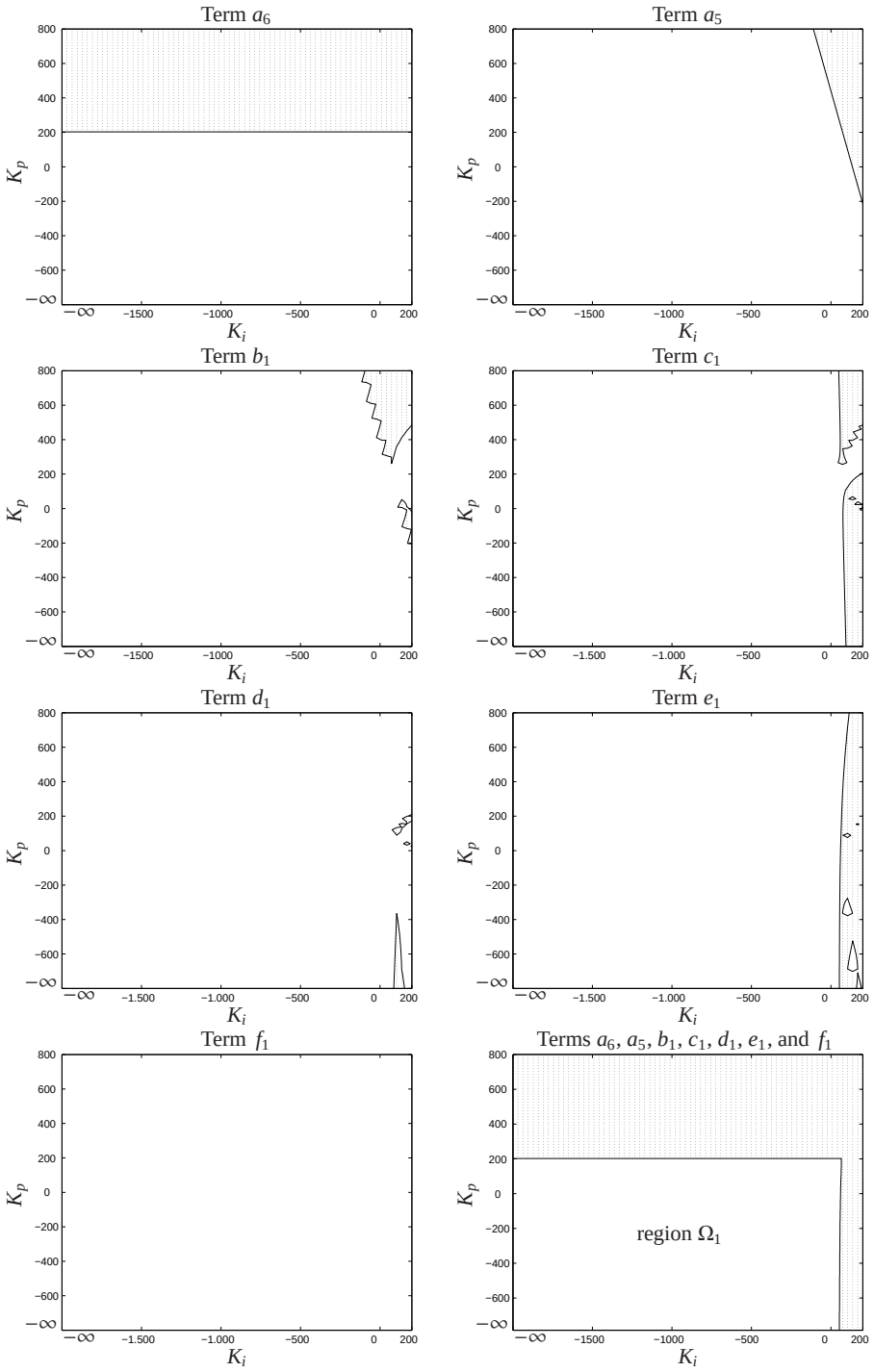

Fig. 6 Stability region Ω_1 obtained from the Routh–Hurwitz stability criterion

Therefore, our objective will be the minimization of the function $\Upsilon\left(K_p, K_i\right)$. Note that by doing this, we are minimizing the effect of the external excitation d on the regulated output y.

Thus, as $\|D\|_\infty$ is a constant value, minimization of $\Upsilon\left(K_p, K_i\right)$ can be formulated as:

$$\min\left(\Upsilon\left(K_p, K_i\right)\right) = \sup_{\omega\in(-\infty,\infty)} |F(jw)| \tag{52}$$

which can be solved by setting the first parcial derivatives of equation (52) to zero. Unfortunately, solution of

$$\frac{\partial\Upsilon\left(K_p, K_i\right)}{\partial K_p} = 0 \tag{53}$$

$$\frac{\partial\Upsilon\left(K_p, K_i\right)}{\partial K_i} = 0 \tag{54}$$

can not be handled analytically as equations (53)-(54) involves a high order polynomials whose roots can not be obtained by analytical methods. However, this minimization process can be handled numerically by computing $\Upsilon\left(K_p, K_i\right)$ inside region Ω_1 and finding the values of parameters K_p and K_i that make function $\Upsilon\left(K_p, K_i\right)$ minimal.

In our case, substitution of polynomials D_p, N_p and N_{p_0} from transfer functions (20)-(21) into (26) lead us to the function $\Upsilon\left(K_p, K_i\right)$ which is illustrated in Figure 7.

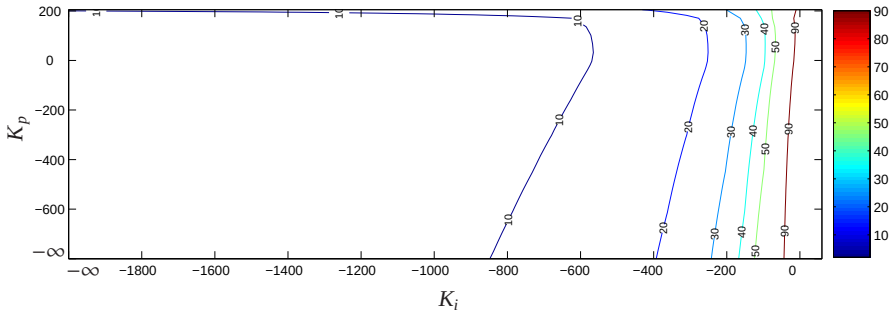

Fig. 7 Variation of $\Upsilon\left(K_p, K_i\right)$ on region Ω_1.

It can be seen how function $\Upsilon\left(K_p, K_i\right)$ is minimized by using $K_{i_{opt}} \to -\infty$. However, this may not be the best solution as the control demand may be unnecessarily increased.

Thus, at this point we look for the pair $(K_i, K_p)_{opt} \in \Omega_1$ such that function $\Upsilon\left(K_p, K_i\right)$ is minimized and the peak of the active control force $f_{c_{\max}}$ is smaller than the maximum MR damper force $f_{\max} = S_f \times f^*_{\max} = 60 \times 3000(\mathrm{N}) = 1.8 \times 10^5(\mathrm{N})$.

To this end, the closed loop system shown in Figure 5 has been simulated numerically for different values of $(K_i, K_p) \in \Omega_1$ with different excitations $d(t)$ which come from some representative earthquake records.
The simulation results provide us with the information about the control effort and the control efectiveness ratio $\|y^c\|_2/\|y^u\|_2$ inside region Ω_1. Variables $\|y^c\|_2$ and $\|y^u\|_2$ correspond to the L_2-norm of the system regulated output for the controlled and uncontrolled cases respectively.

Figure 8 shows region $\Omega_2 \subset \Omega_1$ where $f_{c_{\max}} \leq f_{\max}$ and $\|y^c\|_2/\|y^u\|_2 \leq 0.60$. Hence, we can select the pair $(K_i, K_p)_{opt}$ inside region Ω_2

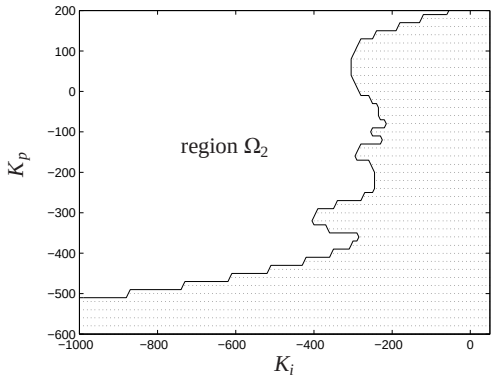

Fig. 8 Region Ω_2.

Figure 8 suggest that the region Ω_2 is unbounded with respect to the parameter K_i. However, choosing large value for this parameter may lead to numerical errors in the computation of the active control law. Hence, it sounds appropriate to have the value of parameter $K_{i_{opt}}$ as small as possible. This selection implies that parameter $K_{p_{opt}}$ is near to the stability limit $K_p \leq 202.3$ obtained from the Routh–Hurwitz stability criterion (see Figure 6). Thus, the closed loop can become unstable in the presence of process parameters uncertainty. For this reason, the criterion to choose parameters $(K_i, K_p)_{opt} \in \Omega_2$ is the robustness of the controller against model uncertainties. This is addressed in what follows.

Robustness of the controller against model uncertainties

The objective of this paragraph is to compute the pair $(K_i, K_p)_{opt} \in \Omega_2$ so that the resulting controller can cope with the uncertainty associated to the plant model (2)-(4). It is necessary to guarantee that closed loop system remains stable when parameters m_i, k_i, and ζ_i, $i = 1, ..., n$ of the structural model vary inside a bounded uncertainty region $\Theta\ (m_i, k_i, \zeta_i)$.

In our analysis the uncertainty region $\Theta\ (m_i, k_i, \zeta_i)$ has been established by taking parameters m_i, k_i, and ζ_i, $i = 1, 2, 3$ as Gaussian distributed with the mean and variance as follows

$$\mu_{m_i} = m_i \quad \mu_{k_i} = k_i \quad \mu_{\zeta_i} = \zeta_i \tag{55}$$

$$\sigma_{m_i} = 0.30 m_i \quad \sigma_{k_i} = 0.30 k_i \quad \sigma_{\zeta_i} = 0.60 \zeta_i. \tag{56}$$

where m, k and ζ come from structural matrices (5), (6) and vector (9) as follows: $k = [42710, 56610, 56610]$ $(\frac{\text{N}}{\text{cm}})$, $m_i = 202.53$ $(\frac{\text{Ns}^2}{\text{cm}})$, and $\zeta = [0.31, 0.62, 0.63]$ (%) for the structure under analysis.

Figure 9 illustrates the variation of the fundamental frequencies f_n and damping ratios ζ when structural parameters vary inside the aforementioned uncertainty region $\Theta\ (m_i, k_i, \zeta_i)$. Red points are the nominal values of the pairs (f_{n_i}, ζ_i) from equations (8) and (9).

Note that variation on parameters m_i, k_i, and ζ_i, $i = 1, 2, 3$ means a variation on the polynomial (30) on which transfer functions (20)-(21) depends. With this in mind, polynomial (30) has been computed for different values of $(K_i, K_p) \in \Omega_2$ and for structural systems obtained from the variation of parameters m_i, k_i, and ζ_i, $i = 1, 2, 3$ according to (55)-(56). As a result, parameter $K_{p_{opt}}$ has been bounded as $K_{p_{opt}} \leq 182.7$ to guarantee stability of the controller inside the uncertainty region $\Theta\ (f_{n_i}, \zeta_i)$ $i = 1, 2, 3$.

Finally, the gains of the PI controller are selected as

$$K_{p_{opt}} = 182 \quad K_{i_{opt}} = -160$$

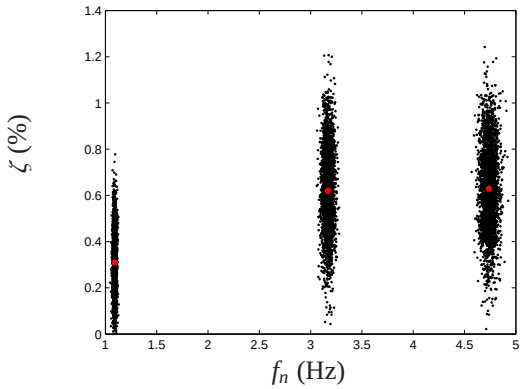

Fig. 9 Uncertainty region $\Theta(f_{n_i}, \zeta_i)$ $i = 1, 2, 3$.

which guarantee system stability, minimization of the closed loop system response and controller robustness against modeling errors are. This result concludes the PI controller design.

Now, it is necessary to design an strategy to induce the MR damper to mimic force f_c as close as possible. This is addressed in what follows.

3.4. Adjusting voltage rule

At this point, note the following: first, due to the nature of the MR damper, it can only reproduce dissipative forces. This means that it can not follows the desired control force f_c unless it is dissipative. Second, inversion of model (10)-(11) is not possible mainly because of the hysteretic nature of the model.

Hence, it sounds convenient to derive an adjusting voltage rule v which takes into account the dissipative nature of the MR damper but avoids model inversion.

Consider the function defined as follows:

$$h(x) = \begin{cases} 0 & \text{if} \quad x \leq 0 \\ V_{\max} & \text{if} \quad x \geq \frac{V_{\max}}{K_v} \\ K_v x & \text{if} \quad 0 \leq x \leq \frac{V_{\max}}{K_v} \end{cases} \tag{57}$$

where K_v is a design parameter and $V_{\max}$ is the maximum input voltage that can be sent to the MR damper. In our case $K_v = 1$ and and $V_{\max} = 5$ (V).

The adjusting voltage rule is chosen in the form

$$v = h\left[(f_c - f)f\right] \tag{58}$$

In this way, the MR damper voltage is modified in order to match f_c only when it is dissipative and $|f_c| > |f|$, otherwise, voltage signal v is set to 0.

Consider now the closed loop of figure 2. It is well know from differential equation theory, that the existence of solutions of $\dot{X} = g(X)$ requires $g(X)$ to be continuous. Hence, continuity of the adjusting voltage rule (58) is required to guarantee the existence of all closed loop solutions in equations (2)-(4) . This is the reason why function h of equation (58) has been introduced instead of the Heaviside function generally used in the literature [16].

4. Control effectiveness

To verify the effectiveness of the control we use the same index terms defined in [33], [34] as detailed in Table 3. Indices J_1 and J_2 describe the control effectiveness on the acceleration

!H

Index	Description
$J_1 = \frac{\max_{t,i}\left(\left\|\ddot{x}^c_{a_i}\right\|_\infty\right)}{\max_{t,i}\left(\left\|\ddot{x}^u_{a_i}\right\|_\infty\right)}$	Normalized peak floor acceleration (L_∞–norm)
$J_2 = \frac{\max_{t,i}\left(\left\|\ddot{x}^u_{a_i}\right\|^c_2\right)}{\max_{t,i}\left(\left\|\ddot{x}^c_{a_i}\right\|_2\right)}$	Normalized peak floor acceleration (L_2–norm)
$J_3 = \max\left(\left\|x^c_1(t)\right\|_\infty\right)$	Fist floor peak displacement
$J_4 = \max\left(\left\|\ddot{x}^c_{a_1}(t)\right\|_\infty\right)$	Fist floor peak absolute aceleration
$J_5 = \max_t\left(\frac{\lvert f(t)\rvert}{W}\right)$	Normalized peak control force
$J_6 = \left(\frac{1}{\tau}\int_0^\tau \lvert f(t)\rvert^2\, dt\right)^{1/2}$	RMS control force

Table 3 Control Index

by comparing the peak acceleration response in terms of L_∞–norm and L_2–norm of the controlled system acceleration $\left\|\ddot{x}^c_{a_i}\right\|_\infty$ and $\left\|\ddot{x}^c_{a_i}\right\|_2$ compared to the uncontrolled system one $\left\|\ddot{x}^u_{a_i}\right\|_\infty$ and $\left\|\ddot{x}^u_{a_i}\right\|_2$. Indices J_3 and J_4 correspond to the L_∞–norm of the displacement and acceleration of the first floor of the controlled system $\left\|x^c_1(t)\right\|_\infty$ and $\left\|\ddot{x}^c_{a_1}(t)\right\|_\infty$. Index J_5 is the maximum force $f(t)$ induced in the device normalized by the weight of the structure $W = 607.59$(kN) and index J_6 refers to the control effort of the real damper.

4.1. Simulation results

Table 4 shows the performance indexes when the structure is controlled by implementing passive–off ($v = 0$ (V)) and passive–on ($v = 5$ (V)) cases, the proposed PI semiactive control and the corresponding active PI control. Performance index results for backstepping and QFT based methods from references[33),(34)] are also provided to have a basis of comparison. External excitations are shown in Figure 10 and come from real records scaled by a factor of 0.4 according to references[33),(34)].

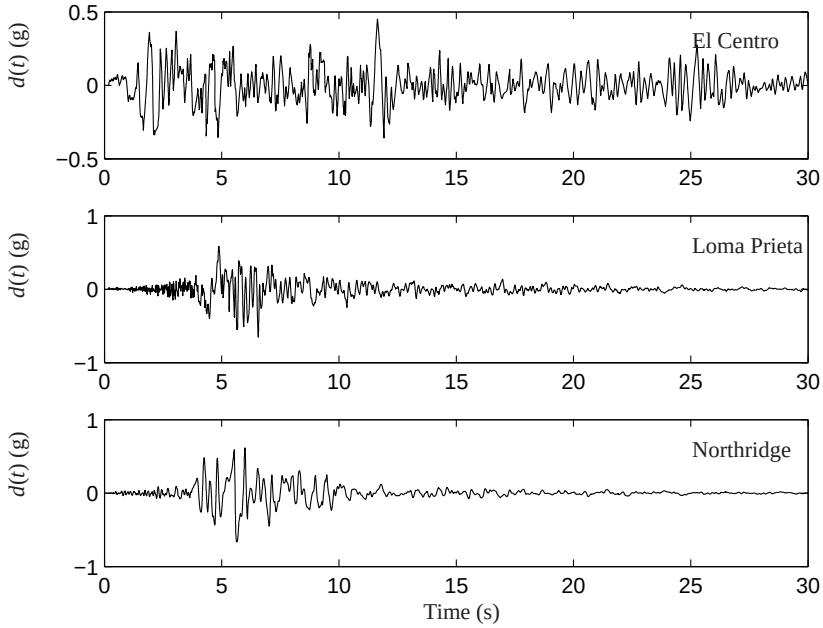

Fig. 10 External excitations $d(t)$: “El Centro”, “Loma Prieta” and “Northridge”

It can be seen how both of the passive systems are able to achieve a reasonable level of performance. However, in the passive–off case the peak of the first floor displacement (index J_3) is greater than that of the other strategies and in the passive–on case the control effort (index

		Index					
Excitation	Control strategy	J_1	J_2	J_3	J_4	J_5	J_6
El Centro	Passive off	0.81	0.71	5.56	3.46	0.01	2772
	Passive on	0.39	0.38	1.93	3.52	0.12	33108
	Active PI control	0.72	0.56	4.26	2.82	0.08	15646
	Semi active PI control	0.51	0.76	2.84	5.13	0.11	17489
	Backstepping	0.55	0.28	3.11	3.40	0.12	20323
	QFT	0.67	0.40	3.36	3.77	0.12	15578
Loma Prieta	Passive off	0.89	0.66	3.73	4.31	0.01	2530
	Passive on	0.43	0.34	1.63	3.54	0.11	27240
	Active PI control	0.74	0.28	3.07	2.57	0.08	7891
	Semi active PI control	0.74	0.54	3.05	5.18	0.11	12352
	Backstepping	0.58	0.34	3.19	3.27	0.12	17314
	QFT	0.92	0.47	3.38	5.25	0.11	10682
Northridge	Passive off	0.97	0.62	6.67	5.06	0.01	2319
	Passive on	0.50	0.32	3.04	4.07	0.12	26806
	Active PI control	0.82	0.39	4.83	3.17	0.10	11307
	Semi active PI control	0.83	0.52	4.62	6.13	0.11	11635
	Backstepping	0.72	0.38	4.61	4.51	0.12	17212
	QFT	0.64	0.42	4.76	5.06	0.11	18145

Table 4 Controller performance index under “El Centro”, “Loma Prieta” and “Northridge” earthquakes

J_5 and J_6) is greater than that of the other strategies. Thus, because the MR damper has the ability to modify its properties dynamically, the performance of the semiactive cases is better than passive ones in the sense that it reduces the displacement and acceleration of the first floor with respect to the passive–off case using significantly smaller control effort than the one associated to the passive–on case.

On the other hand, the designed active PI control system is very effective in reducing the structural responses but this comes at the price of large power requirements to generate the control force. Indeed, the semiactive PI controller achieves performance comparable to the active case at with almost the same control effort; however, it requires only a small fraction of the power required to operate the active control system. In addition, the semiactive PI controller can achieve performance comparable to that of more complex strategies as the QFT and backstepping based techniques.

5. Conclusions

This work has dealt with a new semiactive control strategy which results from a PI controller along with an adjusting voltage rule designed in order to make the MR damper to mimic the active control force as close as possible. The gains of the PI controller have been computed in such a way to guarantee system stability, minimization of the closed loop system response and controller robustness against modeling errors. This semiactive controller is very attractive as it does not require a MR damper model and uses only obtainable acceleration and force measurements making it quite implementable. The numerical results show how this simple control law can achieve performance levels comparable to that of more complex algorithms.

Acknowledgments

This work is supported by through grant DPI2005-08668-C03-01. The first author acknowledges the support of the Spanish Ministry of Science and Education through FPI program.

References

(1) N. Aguirre, F. Ikhouane, J. Rodellar, and R. Christenson. Modeling and identification of large scale magnetorheological dampers. In *Fourth European Conference on Structural Control, St. Petersburg, Russia*, 2008.

(2) K. Astrom and T. Hagglund. *PID Controllers: Theory, design and tuning*. Instrument Society of America, North Carolina, 1995.

(3) A. Bahar. *Hierarchical semiactive control of base isolated structures*. PhD thesis, Technical University of Catalunya, 2009.
(4) S. W. Cho, B. W. Kim, H. J. Jung, and I. W. Lee. Implementation of modal control for seismically excited structures using magnetorheological dampers. *Journal of Engineering mechanics*, 131:177–184, 2005.
(5) R. W. Clough and J. Penzien. *Dynamics of structures*. McGraw–Hill, 1992.
(6) S. J. Dyke and B. F. S. Jr. Seismic response control using multiple MR dampers. In *Proc. of the 2nd Intl. Workshop on Struc. Control, Hong Kong*, 1996.
(7) S. J. Dyke and B. F. S. Jr. A comparison of semi-active control strategies for the MR damper. In *Proc. of the International Conf. on Intelligent Information Systems, IASTED, Bahamas*, 1997.
(8) S. J. Dyke, B. F. S. Jr, M. K. Sain, and J. D. Carlson. Seismic response reduction using magnetorheological dampers. In *Proc. of the IFAC World Congress, San Francisco, CA,*, 1996.
(9) S. J. Dyke, J. B. F. Spencer, M. K. Sain, and J. D. Carlson. Modeling and control of magnetorheological dampers for seismic response reduction. *Journal of Smart Materials and Structures*, 5:565–575, 1996.
(10) E. Gildin. *Model and controller reduction of large-scale structures based on projection methods*. PhD thesis, The University of Texas, 2006.
(11) D. Giraldo, O. Yoshida, S. J. Dyke, and L. Giacosa. Control oriented system identification using era. *Journal of Structural Control and Health Monitoring*, 11:311–326, 2004.
(12) C. T. Huang, C. J. Chou, and L. Z. Chen. An automatic pid controller tuning method by frequency response techniques. *The Canadian Journal Of Chemical Engineering*, 75:596–604, 1997.
(13) F. Ikhouane and S. J. Dyke. Modeling and identifcation of a shear mode magnetorheological damper. *Smart Materials and Structures*, 16:605–616, 2007.
(14) F. Ikhouane and J. Rodellar. *Systems with Hysteresis: Analysis, Identification and Control Using the Bouc-Wen Model*. Chichester, UK: Wiley, 2007.
(15) J. A. Inaudi. Modulated homogeneous friction: a semi-active damping strategy. *Earthquake Engineering and Structural Dynamics*, 26:361–376, 1997.
(16) L. M. Jansen and S. J. Dyke. Semi-active control strategies for the MR damper: comparative study. *Journal of Engineering Mechanics, ASCE*, 126:795–803, 2000.
(17) E. A. . Johnson, J. C. Ramallo, B. F. S. Jr, and M. K. Sain. Intelligent base isolation systems. In *Proceedings 2nd World Conference on Structural Control, Kyoto, Japan*, 1998.
(18) E. A. Johnson and B. Erkusz. Dissipativity and performance analysis of smart dampers via lmi synthesis. *Structural Control and Health Monitoring*, 14:471–496, 2007.
(19) B. F. S. Jr, S. J. Dyke, M. K. Sain, and J. D. Carlson. Phenomenological model for a magnetorheological damper. *Journal of Engineering Mechanics, ASCE*, 123:230–238, 1997.
(20) H. R. Karimi, M. Zapateiro, and N. Luo. Robust mixed h_2/h_∞ vibration control of uncertain structures applied to a base isolated structure. In *Proc. of the 4th European Conference on Structural Control, St. Petersburg, Russia*, 2008.
(21) B. C. Kuo. *Automatic control*. Prentice Hall. New Jersey, 1995.
(22) J. R. Leigh. *Control Theory, 2nd Edition*. IEE Control Series 64. United Kingdom, 2004.
(23) K. C. Lu, C. H. Loh, J. N. Yang, and P. Y. Lin. Decentralized sliding mode control of a building using mr dampers. *Journal of Smart Materials and Structures*, 17, 2008.
(24) N. Luo, R. Villamizar, and J. Vehi. Backstepping control of nonlinear building structures with hysteretic and frictional dynamics. In *European Control Conference, Kos, Greece*, 2007.
(25) Q. P. H. J. L. N. M. Kwok, T. H. Nguyen and B. Samali. Mr damper structural con-

trol using a multi-level sliding mode controller. In *Australian Earthquake Engineering Society Conference (AEES). Albury, Australia*, 2005.

(26) T. H. Nguyen, N. M. Kwok, Q. P. Ha, J. Li, and B. Samali. Adaptive sliding mode control for civil structures using magnetorheological dampers. In *Proc. International Symposium on Automation and Robotics in Constructions.Tokyo,Japan*, 2006.

(27) J. C. Ramallo, E. A. Johnson, and B. F. S. Jr. Smart base isolation systems. *Journal of Engineering Mechanics, ASCE*, 128:1088–1099, 2002.

(28) R. Villamizar. *Robust control of systems subjected to uncertain distubances and actuator dynamics*. PhD thesis, University of Girona, 2005.

(29) R. Villamizar, N. Luo, S. J. Dyke, and J. Vehi. Experimental verification of backstepping controllers for magnetorheological MR dampers in structural control. In *Proceedings of the 13th Mediterranean Conference on Control and Automation, Limassol, Cyprus*, 2005.

(30) R. Villamizar, N. Luo, J. Veh, and J. Rodellar. Semiactive sliding mode control of uncertain base isolated structures with actuator dynamics. In *Proc. of the SPIE 10th Annual International Symposium on Smart Structures and Materials, Warsaw*, 2003.

(31) O. Yoshida and S. Dyke. Seismic control of a nonlinear benchmark building using smart dampers. *Journal of Engineering Mechanics*, 130:386–392, 2004.

(32) H. Yoshioka, J. C. Ramallo, and B. F. S. Jr. Smart base isolation strategies employing magnetorheological dampers. *Journal of Engineering Mechanics*, 128:540–551, 2002.

(33) M. Zapateiro. *Semiactive control strategies for vibration mitigation in adaptronic structures equipped with magnetorheological dampers*. PhD thesis, University of Girona, 2009.

(34) M. Zapateiro, H. R. Karimi, N. Luo, and B. F. S. Jr. Real-time hybrid testing of semiactive control strategies for vibration reduction in a structure with MR damper. *Structural Control and Health Monitoring*, 2009.

(35) M. Zapateiro, N. Luo, and H. R. Karimi. QFT control for vibration reduction in structures equipped with MR dampers. In *American Control Conference, Seattle, W. A, U.S.A.*, 2008.

(36) M. Zapateiro, R. Villamizar, and N. Luo. Semiactive seismic vibration control of structures equipped with magnetorheological dampers. *International Journal of Factory Automation, Robotics and Soft Computing*, 2008.

(37) J. G. Ziegler and N. B. Nichols. Optimum settings for automatic controllers. *Trans. ASME*, 64:759–768, 1942.